The Astrophysical Journal, 690:1105–1111, 2009 January 10 doi:10.1088/0004-637X/690/2/1105

THE MID-INFRARED NARROW-LINE BALDWIN EFFECT REVEALED BY *SPITZER*

Mark Keremedjiev[1], Lei Hao[2,3], and Vassilis Charmandaris[4,5,6]
[1] Department of Astronomy, University of Florida, Gainesville, FL 32611, USA; msk@astro.ufl.edu
[2] Astronomy Department, Cornell University, Ithaca, NY 14853-6801, USA
[3] Department of Astronomy, University of Texas, Austin, TX 78712, USA
[4] Department of Physics, University of Crete, GR-71003, Heraklion, Greece
[5] IESL/Foundation for Research and Technology-Hellas, GR-71110, Heraklion, Greece
[6] Chercheur Associé, Observatoire de Paris, F-75014, Paris, France
Received 2008 June 18; accepted 2008 August 22; published 2008 December 2

ABSTRACT

We present our discovery of a narrow-line Baldwin effect, an anticorrelation between the equivalent width (EW) of a line and the flux of the associated continuum, in 5–20 μm mid-infrared (mid-IR) lines from a sample of 68 active galactic nuclei (AGNs), located at $z < 0.5$, observed with the Infrared Spectrograph on the *Spitzer Space Telescope*. Our analysis reveals a clear anticorrelation between the EW of the [S IV] 10.51 μm, [Ne II] 12.81 μm, and [Ne III] 15.56 μm lines and their mid-IR continuum luminosities, while the Baldwin effect for [Ne V] 14.32 μm is not as obvious. We suggest that this anticorrelation is driven by the central AGN, and not circumnuclear star formation in the host galaxy, and present a new method of analyzing this effect in mid-IR lines. We also find that the slope of the narrow-line Baldwin effect in the mid-IR does not appear to steepen with increasing ionization potential. Examining the dependence of the EW on the Eddington ratio ($L/L_{\rm Edd}$), we find no strong relationship for mid-IR lines. Our study indicates that the narrow-line mid-IR Baldwin effect is quite different from the broad-line optical/UV Baldwin effect, and it is possible that the two effects are unrelated. The anticorrelations discovered open new possibilities in understanding the physics of the ionizing region and the continuum reprocessing by dust.

Key words: galaxies: active – infrared: galaxies – quasars: emission lines

Online-only material: color figures

1. INTRODUCTION

The Baldwin effect, first discovered by Baldwin (1977), reports the decrease of the equivalent width (EW) of the broad C IV 1549 Å line with increasing ultraviolet (UV) luminosity in active galactic nuclei (AGNs). The relationship was initially established with the hope that quasars could be used as potential standard candles in observational cosmology. Extended examination of the relationship over the past decades for both quasars and Seyferts demonstrated that the relationship is not caused by selection effects, but its cosmological use is limited due to large scatter (see the review of Osmer & Shields 1999 and Kinney et al. 1990; Wilkes et al. 1999; Green et al. 2001; Croom et al. 2002; Dietrich et al. 2002; Kuraszkiewicz et al. 2002; Shang et al. 2003).

Significant correlations also exist between the continuum emission and the EW in other UV and optical emission lines including Lyα, Hβ, C IV, C III, Lyβ, O IV, O I, O II, Al III, C III, Mg II, and Si IV + O IV. It was also found that the slope of these relationships appear to increase with increasing ionization potential. In addition, an X-ray Baldwin effect has also been reported in Fe Kα (Iwasawa & Taniguchi 1993; Nandra et al. 1997; Page et al. 2004).

The physical origin of this effect is still not clear. A plausible explanation is the softening of the ionizing continuum shape with increasing L, which would lead to weaker emission lines compared to the local continuum (Baskin & Laor 2004). However, this has been challenged by Wilkes et al. (1999), who found no correlation between any of the UV and optical lines with the X-ray luminosity or X-ray slope. They suggested a model in which limb darkening and the projected surface area of an optically thick, geometrically thin, disk combine to cause the Baldwin effect.

Some have also argued that the Eddington ratio $L/L_{\rm Edd}$, a tracer of AGN accretion, may drive the Baldwin effect (Boroson & Green 1992). The Baldwin effect may then just be a secondary correlation induced by the tendency of more luminous AGNs to have a higher $L/L_{\rm Edd}$ (Baskin & Laor 2004; Shang et al. 2003). Others have argued that the fundamental driver is the mass of the supermassive black hole $M_{\rm BH}$ instead of L or $L/L_{\rm Edd}$ (Warner et al. 2003; 2008). One further plausible explanation is that metallicity of the gas in the AGN affects the EW of the lines in a way that would generate a Baldwin effect (Dietrich et al 2002).

Most of the discussion of the Baldwin effect has focused on broad lines, but few papers have also noticed a narrow-line Baldwin effect (Green et al. 2001; Croom et al. 2002; Boroson and Green 1992). Since the narrow-line region (NLR) in quasars may extend to kpc scales, the physics related to the narrow-line Baldwin effect may be different from those driving the broad-line Baldwin effect (Osmer & Shields 1999), and may simply be due to the covering factor of the NLR (Page et al. 2004). This is manifest in a "disappearing NLR" model, where the NLR size is related to the AGN luminosity and highly-luminous AGN would have a weak or even a nonexistent NLR (Croom et al. 2002).

Complications arise when moving into the mid-IR. Several authors have noted that in many cases, the IR spectra of AGNs do not reflect their optical or UV classifications as reprocessing of the ionizing radiation by the intervening dust and circumnuclear star-formation activity affects the mid-IR spectral features (Lutz et al. 1998; Laurent et al. 2000; Armus et al. 2007; Spoon et al. 2007). As a result, accurately quantifying the

AGN contribution to the IR or bolometric luminosity of dust-enshrouded galaxies is still a largely unanswered problem (see Charmandaris 2008 for a review). Ascertaining the extent of AGN domination in the mid-IR presents unique challenges to determining the extent of a Baldwin effect. We embarked on the detailed study of the effect using *Spitzer* data (Keremedjiev & Hao 2006) while an analysis using ground-based observations with the Very Large Telescope/VLT Imager and Spectrometer in the InfraRed (VLT/VISIR) and comparing to X-ray luminosity has been presented by Hönig et al. (2008).

In this paper, we report on our discovery of a narrow-line Baldwin effect in the mid-IR based on *Spitzer* observations of a large sample, which consists of 68 optically classified AGNs. Our observations and data analysis are presented in Section 2, our results and detected correlations are shown in Section 3, while the implications of those are discussed in Section 4.

2. OBSERVATIONS AND DATA REDUCTION

We compiled a sample of 16 Palomar-Green (PG) Quasars, 33 Seyfert Galaxies, and 19 Two Micron All Sky Survey (2MASS) AGNs with $z < 0.5$ observed with the *Spitzer Space Telescope*'s Infrared Spectrograph (IRS).[7] All objects were observed in the short-high (SH), short-low (SL), and long-low (LL) IRS modules. The low-resolution modules SL (5.2–14.5 μm) and LL (14.0–38.0 μm) have a spectral resolution of 64–128, whereas the high-resolution module SH (9.9–19.6 μm) has a resolution of ~600 (Houck et al. 2004). For this experiment, our effective coverage is limited by the SH bandpass. The data were reduced at the *Spitzer* Science Center (SSC), using data reduction pipeline 13.2. The Basic Calibrated Data (BCD) products from the SSC were used in our analysis.

To obtain the low-resolution spectra, we coadded the images of the same nod position. The background was then subtracted from the coadded image of the other nod position. The mid-IR spectra were extracted from these images with the Spectral Modeling, Analysis, and Reduction Tool (SMART Ver. 5.5.1; Higdon et al. 2004) using a variable width aperture to recover the diffraction-limited point-spread function (PSF).

For high-resolution data, the background cannot be subtracted in the same way as in the low-resolution cases. Due to the limited size of both apertures of IRS high-resolution modules, even point sources tend to fill them, making differencing between the two nods impossible. Thus, images of the same nod position were coadded using median averaging and full aperture extractions were conducted in SMART. The resulting spectra were cosmetically trimmed by eye for order overlap across all orders. This was done to compensate for the low signal-to-noise ratio (S/N) present in most spectra. Unfortunately, separate background observations were not made for our sources, and therefore we cannot apply any background subtraction to our high-resolution data. As a result, the continuum of the high-resolution spectra will always contain a background component.

The spectra were returned to their rest frames using the redshifts of the targets obtained from the NASA Extragalactic Database (NED).[8] The continuum flux was calculated from the local continuum in the low-resolution data. Calculation of the continuum luminosity was done with distances determined from z, where we assumed that a value of 73 km s^{-1} Mpc^{-1} was used for H_0 (Riess et al. 2005).

Line strengths were measured from the high-resolution spectra. Since a significant number of our sources only have SH data (9.9 μm < $\lambda_{\rm SH}$ < 19.6 μm), we will focus on studying the narrow-line Baldwin effect in strong emission lines in the SH wavelength range. More specifically, these lines and their corresponding ionization potential are [S IV] 10.51 μm (47.22 eV), [Ne II] 12.814 μm (40.96 eV), [Ne V] 14.320 μm (126.25 eV), and [Ne III] 15.555 μm (63.42 eV). Line strengths were determined by fitting a Gaussian function to the feature at the central wavelength. The local continuum was subtracted off with a linear fit.

EWs were measured by dividing the line strength measured in high-resolution by the continuum strength measured in low resolution. This was done because the low-resolution data do not contain the background flux present in the high-resolution data, and thus they more accurately reflect the actual continuum flux. In Table 1, we present line strengths, continuum values, and EW for all our objects as well as redshifts and luminosity distances.

3. RESULTS

In Figure 1, we present the EW of the four lines as a function of the nearby mid-IR monochromatic continuum luminosity. A narrow-line Baldwin effect, where EW declines as luminosity increases, appears to manifest itself in all four lines across six orders of magnitude in luminosity. As mentioned earlier, our sample contains both type I (quasars and Seyfert 1s) and type II (mostly Seyfert 2s) AGNs and we include both types in our analysis. In all figures, we indicate type 1 objects with filled red circles and type 2 with open green circles. We do not see any evidence that either type 1 or type 2 AGNs deviate from the trend and while type 2 AGNs are generally in the lower mid-IR luminosity range, they do not skew the overall Baldwin effect. The blue open triangles denote galaxies with significant circumnuclear starburst contribution, classified in a manner described below. We exclude them from further correlation analysis.

In Figure 1, we also include the error bars in our data. The uncertainties in the continuum luminosity were generated by calculating the variance in the local continua. No assumptions were made about uncertainties in the redshift measurements, and therefore our errors are likely lower limits. The flux density uncertainty was a combination of variance in the local high-resolution continuum and error in the profile fitting. Only lines detected with confidence greater than 3$\sigma_{\rm flux}$ were included in our analysis. The error in EW was the propagation of the noise, both in low resolution $\sigma_{\rm continuum}$ and in high resolution $\sigma_{\rm flux}$. For nearly all our data, the uncertainty was <10% indicating good quality of our measurements. The reason why the error bars appear so small on the plot has much to do with the large dynamic range in luminosities and EW measured in our sample.

We used the conventional definition of the Baldwin effect expressed as

$$W_\lambda = \alpha L_\lambda^\beta, \quad (1)$$

where W_λ indicates the EW and β the slope of the anti-correlation. We performed a least-squares fit to the data in logarithmic space and in order to test the linear correlation of the log of EW versus log of luminosity, a Spearman

[7] The IRS was a collaborative venture between Cornell University and Ball Aerospace Corporation funded by NASA through the Jet Propulsion Laboratory and the Ames Research Center.

[8] This research has made use of the NASA/IPAC Extragalactic Database (NED) which is operated by the Jet Propulsion Laboratory, California Institute of Technology, under contract with the National Aeronautics and Space Administration.

Table 1
Various Measured Properties for the Galaxies in Our Sample

Name	z	D_L	[S IV] Flux	[S IV] EW	[S IV] Cont.	[Ne II] Flux	[Ne II] EW	[Ne II] Cont.	[Ne V] Flux	[Ne V] EW	[Ne V] Cont.	[Ne III] Flux	[Ne III] EW	[Ne III] Cont.	5.5 μm Cont.
2MASSJ000703	0.114	482	2.32	0.0361	64.1	2.29	0.0377	60.7	2.69	0.0503	53.4	5.29	0.105	50.5	115
2MASSJ005055	0.136	575	2.32	0.0241	96.3	<1.11	<0.0122	90.8	4.27	0.0500	85.4	N/A	N/A	N/A	170
2MASSJ010835	0.285	1200	<0.6910	<0.0285	24.2	1.66	0.0643	25.8	<0.616	<0.0264	23.3	<1.73	<0.0872	19.8	86.5
2MASSJ015721	0.213	900	<0.6450	<0.00778	83.0	1.57	0.0182	86.3	<0.739	<0.00946	78.1	<0.853	<0.0119	71.5	163
2MASSJ034857	0.140	592	<1.109	<0.00690	161	0.952	0.00595	160	<0.912	<0.00667	137	<0.977	<0.00825	118	570
2MASSJ091848	0.210	887	2.26	0.0264	85.7	0.982	0.0122	80.7	4.48	0.0626	71.7	2.60	0.0396	65.8	198
2MASSJ102724	0.149	630	<0.9020	<0.0131	68.7	<0.740	<0.0113	65.8	<0.971	<0.0165	58.8	<1.22	<0.0218	55.8	161
2MASSJ105144	0.231	976	1.66	0.0671	24.7	1.76	0.0693	25.5	1.61	0.0643	25.0	3.02	0.122	24.7	55.3
2MASSJ130005	0.080	338	<0.878	<0.00357	246	1.67	0.00870	192	<0.706	<0.00432	163	1.45	0.00978	148	526
2MASSJ140251	0.187	790	<0.644	<0.0160	40.3	<0.533	<0.01867	28.7	<0.811	<0.0352	23.1	<0.791	<0.0376	21.0	91.0
2MASSJ145331	0.139	587	<0.600	<0.0158	38.1	4.77	0.0474	101	<0.774	<0.00893	86.7	4.75	0.0649	73.2	295
2MASSJ150113	0.258	1.09e3	<0.617	<0.0148	41.9	<0.746	<0.0187	39.9	<0.797	<0.0219	36.4	N/A	N/A	0	90.3
2MASSJ151653	0.190	803	<0.692	<0.00277	250	<0.722	0.00468	154	<0.717	<0.00587	122	2.19	0.0202	109	534
2MASSJ163700	0.211	892	<0.780	<0.0311	25.0	<0.743	<0.0279	26.7	<0.810	<0.0411	19.7	<1.19	<0.0611	19.4	50.1
2MASSJ165939	0.170	718	2.01	0.0143	141	1.44	0.0119	121	2.43	0.0229	106	4.62	0.0463	99.7	210
2MASSJ171442	0.163	689	<0.623	<0.0165	37.7	1.32	0.0468	28.3	<0.734	<0.0335	21.9	<0.605	< 0.0285	21.2	79.6
2MASSJ222221	0.211	892	<0.706	<0.0116	60.9	<0.578	<0.0129	45.0	0.903	0.0241	37.5	<1.05	<0.0290	36.2	113
2MASSJ222554	0.147	621	<0.605	<0.0157	38.5	0.573	0.0128	44.6	1.02	0.0266	38.2	1.02	0.0300	33.8	98.9
2MASSJ234449	0.199	841	1.25	0.0217	57.8	<0.772	<0.0171	45.2	1.90	0.0477	39.9	2.12	0.0565	37.5	109
3C120	0.033	140	24.7	0.0410	603	8.20	0.0175	468	18.3	0.0411	444	29.9	0.0663	451	990
3C273	0.158	669	3.55	0.00450	788	1.56	0.00279	558	2.85	0.00576	495	5.78	0.0121	480	1.93e3
3C445	0.0562	238	2.39	0.00573	417	2.90	0.00988	293	3.65	0.0149	244	3.82	0.0153	250	791
ESO103-g035	0.0133	56.2	7.35	0.00768	957	20.4	0.0120	1.69e3	11.1	0.00633	1.75e3	23.9	0.0145	1.65e3	1.63e3
Fairall9	0.0470	199	<1.52	<0.00226	674	3.26	0.00648	503	1.71	0.00382	448.6	4.51	0.0106	426	1.07e3
H1846-786	0.0743	314	<1.05	<0.0109	96.2	1.45	0.0163	89.3	<0.716	<0.00770	93.0	1.63	0.0182	89.8	170
IC4329a	0.0161	67.8	22.4	0.0101	2.21e3	21.9	0.0110	1.99e3	25.6	0.0133	1.93e3	42.5	0.0233	1.82e3	3.02e3
IC5135	0.0162	68.2	4.62	0.0118	393	65.3	0.0989	660	9.01	0.0156	578	20.0	0.0329	606	502
IRAS 07145-2914	0.00566	23.9	94.4	0.198	478	50.8	0.0673	756	62.7	0.0727	863	142	0.156	911	648
I Zw 1	0.0611	258	<2.34	<0.00167	1.40e3	2.93	0.00293	1.00e3	2.57	0.00297	863	5.22	0.00630	829	1.88e3
M-6-30-15	0.00775	32.8	7.30	0.0100	730	3.67	0.00572	641	5.08	0.00810	628	6.76	0.0117	578	1.25e3
Mrk1066	0.0120	50.8	10.5	0.0240	439	110	0.141	776	10.0	0.0142	704	46.7	0.0616	759	607
Mrk3	0.0135	57.1	60.6	0.0504	1.20e3	100	0.0612	1.64e3	64.6	0.0357	1.81e3	182	0.0930	1.96e3	1.10e3
Mrk509	0.0344	145	9.24	0.0142	649	12.0	0.0225	535	6.23	0.0127	489	16.8	0.0332	506	1.23e3
NGC1275	0.0176	74.2	1.38	$7.00E-4$	1.96e3	47.6	0.0270	1.76e3	3.07	0.00174	1.77e3	20.3	0.0108	1.88e3	1.08e3
NGC1386	0.0029	12.3	25.9	0.0443	585	15.4	0.0166	925	33.8	0.0376	900	35.4	0.0436	812	1.44e3
NGC2110	0.00779	32.9	6.64	0.0115	580	56.9	0.116	489	5.21	0.0141	371	45.4	0.107	424	845
NGC2273	0.00614	25.9	3.73	0.00660	565	42.8	0.0573	747	4.74	0.00701	676	19.5	0.0291	670	970
NGC3081	0.00798	33.7	33.3	0.0751	444	12.5	0.0239	525	31.5	0.0576	547	35.4	0.0606	584	445
NGC4151	0.00332	14.0	92.7	0.0202	4.58e3	134	0.0328	4.10e3	77.1	0.0195	3.94e3	204	0.0510	4.00e3	7.07e3
NGC4388	0.00842	35.6	53.9	0.112	480	81.2	0.0913	889	46.0	0.0491	938	98.0	0.103	953	1.04e3
NGC4507	0.00842	35.6	9.40	0.00796	1.18e3	33.5	0.0315	1.06e3	10.6	0.00992	1.07e3	32.1	0.0301	1.07e3	2.33e3
NGC4939	0.0104	43.9	18.7	0.212	88.2	7.74	0.0693	112	12.2	0.104	117	25.3	0.188	134	105
NGC4941	0.0037	15.6	8.77	0.0658	133	14.7	0.0976	150	8.21	0.0509	161	22.4	0.124	181	157
NGC5135	0.0137	58.0	12.3	0.0215	573	93.0	0.0986	942	12.3	0.0174	708	41.3	0.0588	702	619
NGC5347	0.00779	32.9	<1.49	<0.00268	556	5.19	0.00812	638	2.01	0.00322	625	4.43	0.00733	605	486
NGC5506	0.00618	26.1	37.8	0.0219	1.73e3	48.4	0.0184	2.64e3	28.1	0.0113	2.50e3	69.7	0.0316	2.20e3	5.75e3
NGC5548	0.0172	72.6	4.42	0.00849	520	9.13	0.0202	453	4.13	0.00965	428	9.89	0.0232	426	558
NGC5643	0.00400	16.9	23.2	0.0410	566	40.3	0.0455	887	25.4	0.0297	855	55.0	0.0615	895	561
NGC7172	0.00868	36.7	4.99	0.0363	138	33.0	0.0762	433	8.63	0.0270	320	16.5	0.0671	246	1.05e3
NGC7213	0.00595	25.1	<1.26	<0.00182	690	25.4	0.0578	439	<0.878	<0.00225	390	12.9	0.0311	416	871
NGC7314	0.00476	20.1	17.3	0.120	144	9.89	0.0483	205	16.4	0.0773	212	20.9	0.100	209	230
NGC7469	0.0163	69.0	9.65	0.00465	2.07e3	207	0.0883	2.34e3	15.0	0.00740	2.02e3	34.8	0.0162	2.15e3	2.08e3
PG0804+761	0.100	423	2.16	0.00529	408	<0.521	<0.00222	235	<0.456	<0.00250	182	1.31	0.00739	177	840
PG1119+120	0.0502	212	2.21	0.00948	233	0.613	0.00315	195	2.19	0.0126	174	2.80	0.0164	171	296
PG1211+143	0.0809	342	<0.676	<0.00139	487	<0.445	<0.00134	332	1.39	0.00478	291	1.13	0.00394	285	849
PG1351+640	0.0882	373	2.49	0.00494	503	2.59	0.00869	298	<0.607	<0.00222	274	3.28	0.0110	300	427
PG1501+106	0.0364	154	9.02	0.0200	451	4.43	0.0104	427	9.00	0.0222	406	12.6	0.0311	406	596
PG2130+099	0.0630	266	4.37	0.0108	404	1.93	0.00576	336	3.80	0.0131	291	6.19	0.0226	274	787
PG0838+770	0.131	554	<0.260	<0.00319	81.6	<0.458	<0.00701	65.4	<0.401	<0.00664	60.3	<0.984	<0.0160	61.4	116
PG1302-102	0.278	1180	2.15	0.0151	142	<0.349	<0.00295	118	0.480	0.00439	109	<0.851	<0.00347	245	174
PG1411+442	0.0896	379	1.10	0.00421	262	<0.306	<0.001780	172	0.964	0.00676	143	1.10	0.00851	129	530
PG1426+015	0.0865	365	1.75	0.00630	277	1.23	0.00615	200	1.44	0.00809	178	2.63	0.0154	171	505
PG1440+356	0.0791	334	1.73	0.00848	204	4.52	0.0286	158	1.83	0.0137	133	3.74	0.0279	134	685

Table 1
(Continued)

Name	z	D_L	[S IV] Flux	[S IV] EW	[S IV] Cont.	[Ne II] Flux	[Ne II] EW	[Ne II] Cont.	[Ne V] Flux	[Ne V] EW	[Ne V] Cont.	[Ne III] Flux	[Ne III] EW	[Ne III] Cont.	5.5 μm Cont.
PG1613+658	0.129	545	1.31	0.00525	250	4.39	0.0236	186	2.33	0.0143	162	3.83	0.0240	159	488
PG1626+554	0.133	562	<0.179	<0.00330	54.4	<0.130	<0.00477	27.2	0.401	0.0183	22.0	<0.157	<0.00772	20.4	115
PG2214+139	0.0658	278	0.724	0.00321	226	1.26	0.00894	141	<0.424	<0.00391	109	0.781	0.00756	103	522
PG2251+113	0.326	1380	0.854	0.0126	67.8	<0.268	<0.00515	52.0	0.868	0.00710	122	5.58	0.0254	220	161
PG2349-014	0.174	735	1.88	0.0197	95.7	1.76	0.0215	81.9	0.938	0.0114	82.3	2.53	0.0305	83.1	205

Note. D_L is given in Mpc, fluxes are in (10^{-21} W cm^{-2}), EWs are measured in (μm), and continuum values are measured in (10^{-21} W cm^{-2} μm^{-1}).

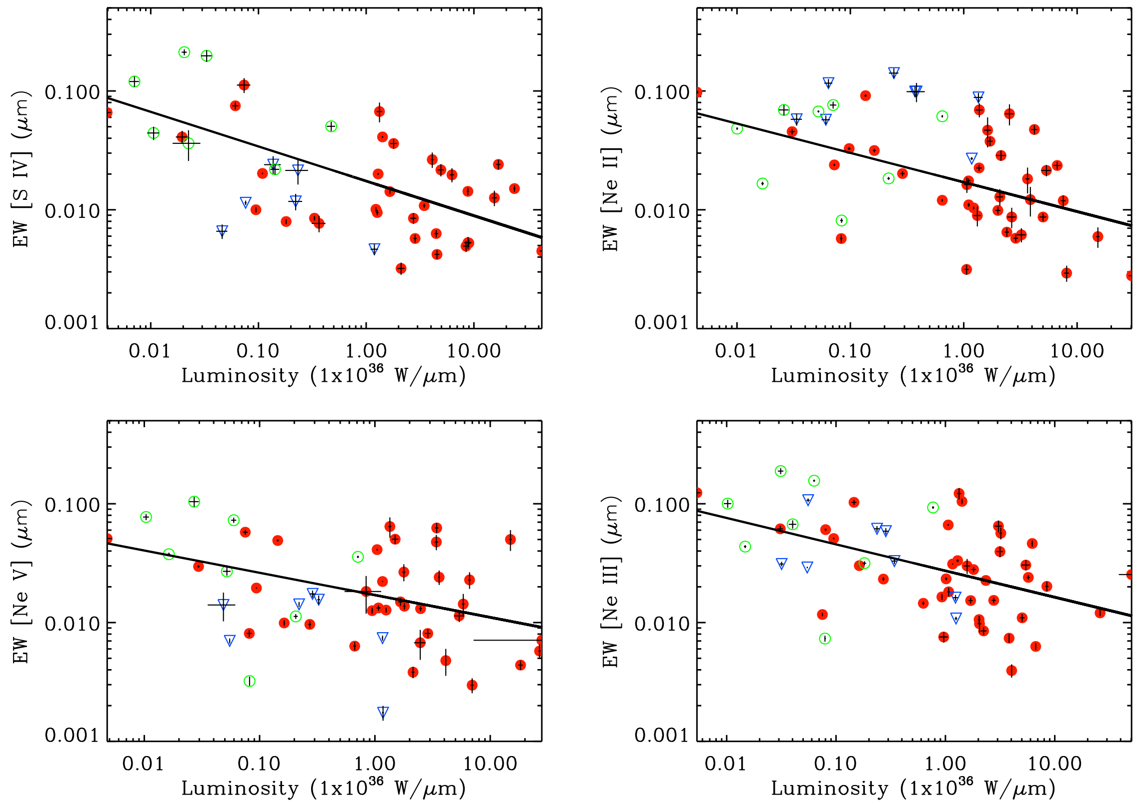

Figure 1. Plots of the EW of [S IV], [Ne II], [Ne V], and [Ne III] as a function of the continuum monochromatic luminosity next to the line. The green open circles denote Seyfert 2 galaxies while the red filled circles indicate the Seyfert 1 galaxies. Starburst galaxies are marked in blue open triangles. The data are overplotted with lines representing the least-squares fits.

(A color version of this figure is available in the online journal.)

rank correlation was employed. The best fits to the data are also plotted in Figure 1.

In three lines, [S IV], [Ne II], and [Ne III] we find a greater than 3σ significance in the anticorrelation. For [S IV], the Spearman rank correlation strength is -0.60 with a null-hypothesis value of 4.16×10^{-5}. The scatter is comparable to the C IV Baldwin effect (Kinney et al. 1990) and the least-squares slope is -0.29 ± 0.05, steeper than the C IV Baldwin effect which is near -0.17 (Kinney et al. 1990; Wilkes et al. 1999; Osmer & Shields 1999; Laor et al 1995). The [Ne II] anticorrelation also manifests itself with a Spearman rank value of -0.48, significance of 8.88×10^{-4}, and a slope of -0.25 ± 0.06. For [Ne III], the correlation is -0.46, significance is 1.17×10^{-3}, and slope is -0.22 ± 0.06.

The significance of these correlations was tested in two different ways. The first was by calculating the number of deviations from the null-hypothesis value for the Spearman rank coefficient. The second was by running Monte Carlo simulations where we randomly assigned our EW values to our continuum measurements. This was done 100,000 times for each line, and the resulting correlations were noted. In all cases where we claim to have a greater than $>3\sigma$ significance, the Monte Carlo simulations provided a second, independent verification.

Unlike the first three lines, when we examine the [Ne V] line, we find that the correlation strength is just -0.41 (5.34×10^{-3} significance) with a slope of -0.19 ± 0.06. The 2.5σ significance and low-correlation value are considered marginal. As we will discuss in the following sections, this was rather unexpected since [Ne V], due to its high excitation potential, is a telltale sign of AGN activity. Since the Baldwin effect is, at least in the optical/UV, directly coupled with the AGN activity, one would expect that it would be more prominent in strong mid-IR AGN lines as well.

3.1. Eddington Luminosities

In order to examine the possibility of the Eddington ratio ($L/L_{\rm Edd}$) as a driver for the mid-IR narrow-line Baldwin effect, we searched the literature and calculated $L/L_{\rm Edd}$ for 29 of our sources that had measured bolometric luminosities and black-hole masses. We obtained $L/L_{\rm Edd}$ for our targets from Czerny et al. (2001), McHardy et al. (2005), Panessa et al. (2006), Vestergaard & Peterson (2006), and Woo & Urry (2002).

Our analysis revealed no strong relationship between Eddington Luminosity and EWs for mid-IR lines. The Spearman rank correlation values, which we found, are −0.21 for [S IV], −0.45 for [Ne II], −0.36 for [Ne V], and −0.36 for [Ne III]. Their corresponding null-hypothesis values are 0.320, 0.032, 0.070, and 0.063, respectively. The low-correlation values coupled with the fact that none of relations have $>3\sigma$ significance indicates that the Eddington ratio is not a driving factor for the weakening of lines in the NLR.

3.2. Slopes of the Baldwin Effect

Previous studies of the broad-line Baldwin effect have revealed that as the ionization potential increases, the steepness of the anticorrelation also increases (Osmer & Shields 1999, Wu et al. 1983; Kinney et al. 1987, 1990; Baldwin et al. 1989; Zheng et al. 1995; Dietrich et al 2002). This was first noticed in the comparisons between low ionization lines such as Mg II and Lyα and high ionization lines such as C IV and O VI.

To examine the relationship between the slope and ionization potential in our study, we have compiled a list of β slopes from the literature (Kinney et al. 1990; Zheng et al. 1995; Dietrich et al. 2002; Croom et al. 2002) and also included data from our sample. The result is given in Figure 2, and it demonstrates that the values from our narrow-line study of AGNs in the mid-IR do not appear to confirm the earlier assessment that the broad-line slope of the Baldwin effect becomes steeper when one considers lines of increasing ionization potential. Further confirmation of this finding is given by Hönig et al. (2008), who presented anticorrelations between mid-IR EWs and 2–10 keV luminosity. They found that the steepness of their anticorrelations was also independent of ionization potentials.

Compared to narrow-line optical data, the results are inconclusive. Croom et al. (2002) only reported strong anticorrelations for two lines, [Ne V] and [O II] (plotted as blue, open diamonds in Figure 2), but felt that [O II] might be contaminated by host galaxy emission. Therefore, there are not enough data points to draw definitive conclusions. They suspected that optical, narrow-line slopes steepen with ionization potential and, if so, then the physical processes driving mid-IR narrow lines may be quite different from their optical counterparts.

4. DISCUSSION

In the original Baldwin effect, the EW of the lines was anticorrelated with the strength of the UV continuum emission, and the latter was used as a tracer of the AGN intensity. This technique is not as direct in the mid-IR because the local continuum may not reflect AGN intensity and could introduce some scatter in the correlations we present in Figure 1. It is well known that in the IR, the spectral signatures of an AGN can be severely blended by emission originating from circumnuclear starbursts (see Laurent et al. 2000; Armus et al. 2007 and references therein). This is only partially due to limited spatial resolution of infrared telescopes and focal plane arrays. More importantly, it is the intervening dust which fully reprocesses the

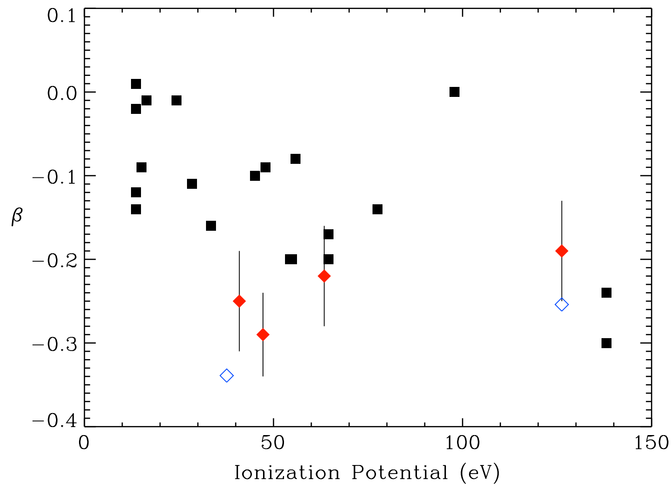

Figure 2. Plot of the ionization potential vs. anticorrelation slope, β. The red filled diamonds denote narrow-line data from this paper and have their associated error bars. The blue open diamonds are narrow-line data from Croom et al. (2002) and black squares are points taken from various sources and represent broad-line data.

(A color version of this figure is available in the online journal.)

intrinsic radiation from the sources—both massive stars and/or an accretion disk—and re-emits it in the IR. This may lead to a difference between the optical and mid-IR classification of a source. To address this issue, a number of diagnostic methods have been developed over the years in order to obtain a robust AGN/starburst classification of mid-IR spectra (see Lutz et al. 1998; Laurent et al. 2000; Armus et al. 2007; Spoon et al. 2007; Charmandaris 2008, Nardini et al. 2008).

It is important for our analysis to explore whether the observed anticorrelation we find is indeed related to the strength of the AGN. Ideally, one could address this by examining the correlation between the line EW and the strength of the X-ray emission (see Hönig et al. 2008). However, these data are not available for our sample so, instead, one can examine how strongly the AGN contributes to the mid-IR continuum emission near the lines versus how much is contaminated by circumnuclear star formation.

It is widely believed that [Ne V] 14.32 μm, due to its high ionization potential, originates in the NLR (see Gorjian et al. 2007 and references therein). So one would have to examine whether most of the emission from [Ne II], [Ne III], and [S IV] in AGNs also come from the same region. Gorjian et al. (2007) found that both the [Ne V] 14.32 μm and [Ne III] 15.6 μm are strongly correlated and deduced that the two must be produced in the same region. Testing the correlation between [Ne V] and [Ne III] in our sample confirms these results at a $>5\sigma$ confidence level. We also examined whether [S IV] and [Ne II] correlate with [Ne V] and found that as with [Ne III], both possessed $>5\sigma$ relationship with very little scatter. Altogether, this suggests that the four lines investigated in this paper are likely to arise from the same region.

To estimate the contribution of massive star formation in the circumnuclear regions of the AGN sampled by the IRS slits, we used two diagnostics which have been proposed by Genzel et al. (1998) and have also been applied by Armus et al. (2007) in a study of local ultraluminous IR galaxies. The first diagnostic was to use the [Ne V]/[Ne II] ratio. This ratio is useful because it is very difficult for stellar sources to produce a significant number of photons capable of ionizing [Ne V]. As a result a

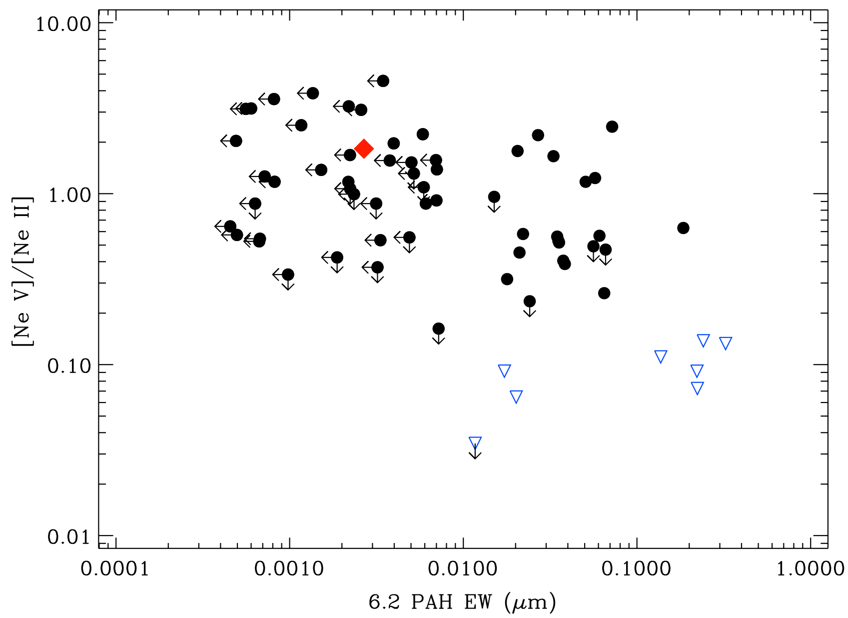

Figure 3. The EW of the 6.2 μm PAH feature vs. [Ne v]/[Ne ii]. The red diamond indicates 3C273, a well-known quasar, where an AGN dominates its mid-IR spectrum (Hao et al. 2005). The blue open triangles denote objects with both high PAH emission and a low neon ratio. These are the strongest candidate starburst galaxies and were flagged as such in our sample.

(A color version of this figure is available in the online journal.)

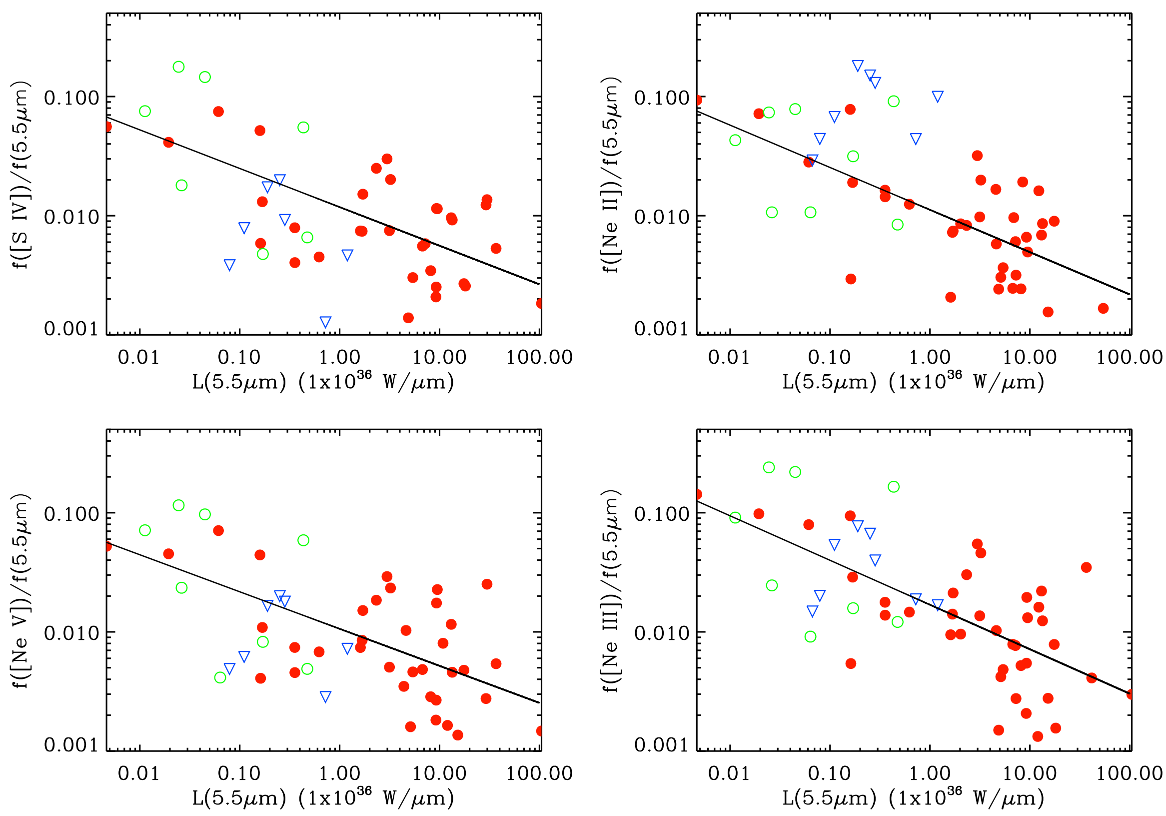

Figure 4. Plot of line flux divided by 5.5 μm flux vs. 5.5 μm luminosity for [S iv], [Ne ii], [Ne v], and [Ne iii]. The green open circles denote Seyfert 2 galaxies while the red filled circles denote Seyfert 1 galaxies. Starburst galaxies are plotted as open blue triangles. The lines representing the best least-squares fits are overplotted.

(A color version of this figure is available in the online journal.)

high [Ne v]/[Ne ii] line ratio indicates the presence of an AGN, which is dominant in the mid-IR (Lutz et al. 1998).

A second diagnostic is to use the EW of the 6.2 μm emission feature. When this feature is strong, it indicates the presence of polycyclic aromatic hydrocarbons (PAHs), which are mainly produced in photodissociation regions (PDRs) when they are excited by the adjacent star-forming regions. Therefore, in Figure 3, we plot the EW (6.2 μm) versus [Ne v]/[Ne ii] similar to Figure 5 of Armus et al. (2007). From Figure 3, we see that there are eight galaxies (NGC 7469, IC 5135, NGC 5135, Mrk1066, NGC 1275, NGC 2110, NGC 2273, and NGC 7213) that have both a low [Ne v]/[Ne ii] value and strong PAH emission. As mentioned before, we flagged them as starburst galaxies and did not use them in our correlation analysis.

Even after removing the most flagrant starburst contaminants, it is evident that Figure 1 still possesses a scatter. This is largely due to the fact that star-formation activity is not a binary phenomenon where it is either overwhelmingly dominant or completely dormant. The Armus et al. (2007) and Genzel et al. (1998) figures show that the diagnostics used are continuous between the two extremes and demonstrate that while there are cases where star formation or the AGN activity dominate, in many galaxies the signature of both in the mid-IR is of similar strength. Therefore, even though we removed the galaxies where we were certain that starburst activity dominated, the remaining classified as AGNs still possess some scatter in our anticorrelations. This is very likely one of the reasons why our [Ne V] result is not strong.

It is evident from the figures that the two diagnostics used are continuous between the two extremes and demonstrate that while there are cases where star formation or the AGN activity dominate, in many galaxies the signature of both in the mid-IR is of similar strength. Therefore, even though we removed the galaxies where we were certain that starburst activity dominated, the remaining classified as AGNs still possess some scatter in our anticorrelations. This is very likely one of the reasons why our [Ne V] result is not strong.

To reduce the possible contribution of star formation to the observed correlations yet further, we removed the local continuum from the analysis altogether. Laurent et al. (2000) and Nardini et al. (2008) pointed out that the 5.5 μm continuum is dominated by emission from dust located near the AGN torus, which heated to near-sublimation temperatures, with minimal contribution from star-formation activity or stellar photospheric emission. Since the flux of a mid-IR line is independent of local continuum levels, the ratio of the line flux to the 5.5 μm continuum versus 5.5 μm luminosity should mitigate continuum contamination altogether.

The result of this experiment is clear. The overall anticorrelations are better than those of Figure 1. All four lines display $>3\sigma$ significance and [Ne II] and [Ne III] actually have $>4\sigma$ significance. The correlation values are -0.58 for [S IV], -0.65 for [Ne II], -0.57 for [Ne V], and -0.62 for [Ne III], with null hypothesis values of 1.03×10^{-4}, 1.29×10^{-6}, 6.41×10^{-5}, and 3.16×10^{-6}, respectively. Using this method, the slope values are -0.32 ± 0.06 for [S IV], -0.36 ± 0.05 for [Ne II], -0.31 ± 0.06 for [Ne V], and -0.37 ± 0.06 for [Ne III], respectively. As expected, the starburst galaxies show some of the strongest [Ne II] emission in our sample and are obvious outliers. The figure further suggests that the anticorrelation is present in all four lines and is driven by the central AGN. The relationship probably only weakened by star formation in the host galaxy. These results are more meaningful than those of Figure 1 principally because of the inclusion of the [Ne V] line which, as mentioned before, we most expect to exhibit a Baldwin effect due to its close relation to the central AGN. Therefore, its inclusion in this analysis points to the AGN as the central driver of this effect. The analysis used in Figure 4 is shown to be a robust way to measure the decrease in line strength with increasing AGN power and may be a better diagnostic tool than the traditional analysis used in Figure 1 for mid-IR lines.

Altogether, our data support the possibility that the driver of the narrow-line Baldwin effect is a dynamic covering factor of the NLR. If this factor changes as a function of AGN luminosity where more luminous AGNs tend to drive the NLR outward, then it would explain the decrease in relative lines' strength with increasing AGN power seen in Figures 1 and 4.

We would like to thank our anonymous referee for carefully examining our manuscript and providing suggestions, which greatly improved it, as well as Fred Hamann for his insightful comments on the paper and for taking the time to revise the work. Dan Weedman was also very helpful in putting together this paper. V.C. would like to acknowledge partial support from the EU ToK grant 39965. This work is based on observations made with the *Spitzer Space Telescope*, which is operated by the Jet Propulsion Laboratory, California Institute of Technology, under NASA contract 1407. Support for this work by the IRS GTO team at Cornell University was provided by NASA through contract 1257184 issued by JPL/Caltech.

REFERENCES

Armus, L., et al. 2007, ApJ, 656, 148
Baldwin, J. A. 1977, ApJ, 214, 679
Baldwin, J. A., Wampler, E. J., & Gaskell, C. M. 1989, ApJ, 338, 630
Baskin, A., & Laor, A. 2004, MNRAS, 350, 31
Boroson, T. A., & Green, R. F. 1992, ApJS, 80, 109
Charmandaris, V. 2008, Infrared Diagn. Galaxy Evol., 381, 3
Croom, S. M., et al. 2002, MNRAS, 337, 275
Czerny, B., Nikolajuk, M., Piasecki, M., & Kuraszkiewicz, J. 2001, MNRAS, 325, 865
Dietrich, M., et al. 2002, ApJ, 581, 912
Genzel, R., et al. 1998, ApJ, 498, 579
Green, P. J., Forster, K., & Kuraszkiewicz, J. 2001, ApJ, 556, 727
Gorjian, V., Cleary, K., Werner, W. M., & Lawrence, C. R. 2007, ApJ, 655, L73
Hao, L., et al. 2005, ApJ, 625, L75
Higdon, S. J. U., et al. 2004, PASP, 116, 975
Hönig, S. F., Smette, A., Beckert, T., Horst, H., Duschl, W., Gandhi, P., Kishimoto, M., & Weigelt, G. 2008, A&A, 485, L21
Houck, J. R., et al. 2004, ApJS, 154, 18
Iwasawa, K., & Taniguchi, Y. 1993, ApJ, 413, 15
Keremedjiev, M., & Hao, L. 2006, BAAS, 38, 1096
Kinney, A. L., Huggins, P. J., Glassgold, A. E., & Bregman, J. N. 1987, ApJ, 314, 145
Kinney, A. L., Rivolo, A. R., & Koratkar, A. P. 1990, ApJ, 357, 338
Kuraszkiewicz, J. K., et al. 2002, ApJS, 143, 257
Laurent, O., et al. 2000, A&A, 359, 887
Lutz, D., et al. 1998, ApJ, 505, L103
McHardy, I. M., Gunn, K. F., Uttley, P., & Goad, M. R. 2005, MNRAS, 359, 1469
Nardini, E., Risaliti, G., Salvati, M., Sani, E., Imanishi, M., Marconi, A., & Maiolino, R. 2008, MNRAS, 385, L130
Nandra, K., George, I. M., Mushotzky, R. F., Turner, T. J., & Yaqoob, T. 1997, ApJ, 488, 91
Osmer, P. S., & Shields, J. C. 1999, ASPC, 162, 235O
Page, K. L., Turner, M. J. L., Done, C., O'Brien, P. T., Reeves, J. N., Sembay, S., & Stuhlinger, M. 2004, MNRAS, 349, 57
Panessa, F., et al. 2006, A&A, 455, 173
Riess, A. G., et al. 2005, ApJ, 627, 579
Shang, H., et al. 2003, ApJ, 586, 52
Spoon, H. W. W., et al. 2007, ApJ, 654, L49
Vestergaard, M., & Peterson, B. M. 2006, ApJ, 641, 689
Warner, C., Hamann, F., & Dietrich, M. 2003, ApJ, 596, 72
Warner, C., et al. 2008, ApJ, submitted
Wilkes, B. J., Kuraszkiewicz, J., Green, P. J., Mathur, S., & McDowell, J. C. 1999, ApJ, 513, 76
Woo, J. H., & Urry, C. M. 2002, ApJ, 579, 530
Wu, C.-C., Boggess, A., & Gull, T. R. 1983, ApJ, 266, 28
Zheng, W., Kriss, G. A., & Davidsen, A. F. 1995, ApJ, 440, 606